


Loss of ADAR1 in macrophages in combination with interferon gamma suppresses tumor growth by remodeling the tumor microenvironment

Weiwei Lin,¹ Yikai Luo,^{2,3} Jie Wu,¹ Haowan Zhang,¹ Ge Jin,¹ Chahua Guo,¹ Hang Zhou,¹ Han Liang ,^{3,4} Xiaoyan Xu¹

To cite: Lin W, Luo Y, Wu J, *et al.* Loss of ADAR1 in macrophages in combination with interferon gamma suppresses tumor growth by remodeling the tumor microenvironment. *Journal for ImmunoTherapy of Cancer* 2023;**11**:e007402. doi:10.1136/jitc-2023-007402

► Additional supplemental material is published online only. To view, please visit the journal online (<http://dx.doi.org/10.1136/jitc-2023-007402>).

Accepted 18 September 2023



© Author(s) (or their employer(s)) 2023. Re-use permitted under CC BY-NC. No commercial re-use. See rights and permissions. Published by BMJ.

For numbered affiliations see end of article.

Correspondence to

Dr Han Liang;
hliang1@mdanderson.org

Dr Xiaoyan Xu;
xyxu@cmu.edu.cn

ABSTRACT

Background ADAR1, the major enzyme for RNA editing, has emerged as a tumor-intrinsic key determinant for cancer immunotherapy efficacy through modulating interferon-mediated innate immunity. However, the role of ADAR1 in innate immune cells such as macrophages remains unknown.

Methods We first analyzed publicly accessible patient-derived single-cell RNA-sequencing and perturbed RNA sequencing data to elucidate the ADAR1 expression and function in macrophages. Subsequently, we evaluated the combined effects of ADAR1 conditional knockout in macrophages and interferon (IFN)- γ treatment on tumor growth in three distinct disease mouse models: LLC for lung cancer, B16-F10 for melanoma, and MC38 for colon cancer. To gain the mechanistic insights, we performed human cytokine arrays to identify differentially secreted cytokines in response to ADAR1 perturbations in THP-1 cells. Furthermore, we examined the effects of ADAR1 loss and IFN- γ treatment on vessel formation through immunohistochemical staining of mouse tumor sections and tube-forming experiments using HUVEC and SVEC4-10 cells. We also assessed the effects on CD8⁺ T cells using immunofluorescent and immunohistochemical staining and flow cytometry. To explore the translational potential, we examined the consequences of injecting ADAR1-deficient macrophages alongside IFN- γ treatment on tumor growth in LLC-tumor-bearing mice.

Results Our analysis on public data suggests that ADAR1 loss in macrophages promotes antitumor immunity as in cancer cells. Indeed, ADAR1 loss in macrophages combined with IFN- γ treatment results in tumor regression in diverse disease mouse models. Mechanistically, the loss of ADAR1 in macrophages leads to the differential secretion of key cytokines: it inhibits the translation of CCL20, GDF15, IL-18BP, and TIM-3 by activating PKR/EIF2 α signaling but increases the secretion of IFN- γ through transcriptional upregulation and interleukin (IL)-18 due to the 5'UTR uORF. Consequently, decreased CCL20 and GDF15 and increased IFN- γ suppress angiogenesis, while decreased IL-18BP and TIM-3 and increased IL-18 induce antitumor immunity by enhancing cytotoxicity of CD8⁺ T cells. We further demonstrate that combination therapy of injecting ADAR1-deficient macrophages and IFN- γ effectively suppresses tumors in vivo.

WHAT IS ALREADY KNOWN ON THIS TOPIC

- ⇒ ADAR1 stands out as the primary adenosine deaminases acting on RNA enzyme responsible for the majority of A-to-I RNA editing occurrences in human cells.
- ⇒ Recently, ADAR1 has emerged as a pivotal factor influencing the outcomes of immune checkpoint blockade therapies by suppressing the sensing of interferon (IFN)-inducible double-stranded RNAs.

WHAT THIS STUDY ADDS

- ⇒ When ADAR1 loss is coupled with IFN- γ treatment in macrophages, it manifests as tumor regression across diverse mouse models.
- ⇒ The synergy between ADAR1 loss in macrophages and IFN- γ administration orchestrates distinct regulation of pivotal cytokines, accomplished through the heightened activation of PKR/EIF2 α signaling.
- ⇒ Concomitant ADAR1 loss in macrophages and IFN- γ treatment elicits a reduction in angiogenesis.
- ⇒ Through the combination of ADAR1 loss in macrophages and IFN- γ treatment, a CD8⁺ T cell-dependent antitumor immunity is induced.
- ⇒ The injection of ADAR1-deficient macrophages alongside IFN- γ treatment effectively inhibits tumor growth in vivo.

HOW THIS STUDY MIGHT AFFECT RESEARCH, PRACTICE OR POLICY

- ⇒ This study provides a comprehensive elucidation of how ADAR1 loss within macrophages contributes to the establishment of an antitumor microenvironment.
- ⇒ Our findings underscore the promising therapeutic prospects of targeting ADAR1 beyond the scope of cancer cells.

Conclusion This study provides a comprehensive elucidation of how ADAR1 loss within macrophages contributes to the establishment of an antitumor microenvironment, suggesting the therapeutic potential of targeting ADAR1 beyond the scope of cancer cells.

INTRODUCTION

Adenosine deaminases acting on RNA (ADARs) are a group of enzymes that bind double-stranded RNAs (dsRNAs) and catalyze the deamination of adenosine (A) to inosine (I), thereby inducing widespread A-to-I RNA modifications in the transcriptome.¹ In humans, ADAR1 (gene symbol: *ADAR*) is the major ADAR enzyme responsible for most RNA editing events; and previous studies of ours and others^{2–4} show that some ADAR1-mediated RNA editing events can induce critical amino acid changes in cancer cells, and like “driver mutations”, they contribute to tumorigenesis and affect drug responses. More recently, ADAR1 has emerged as a key determinant of response to immune checkpoint blockade (ICB) therapies by suppressing the sensing of interferon (IFN)-inducible dsRNAs. When ADAR1 is lost or inhibited in tumor cells, A-form dsRNA sensors such as MDA-5 and PKR are activated and result in an IFN-dependent anti-tumor immune response, thereby enhancing responsiveness to ICBs.^{5–7} Depletion of ADAR1 can also activate Z-form dsRNA sensor ZBP1 and inflammatory cell death.^{8,9} These studies collectively provide a strong rationale for increasing the immune responsiveness of ICB-resistant tumors by targeting tumor-intrinsic ADAR1. Currently, ADAR1 inhibitors are under intensive preclinical and clinical investigations.^{5,6}

Although nominated as an innate immune checkpoint through tumor-intrinsic functions, the role of ADAR1 in innate immune cells remains largely unknown. Within the tumor microenvironment, tumor-associated macrophages (TAM) wield a more prominent influence than any other innate immune population.¹⁰ Macrophages not only affect angiogenesis,^{11,12} a hallmark for cancer development¹³ but also influence the function of T cells, essential players in cancer immunotherapy, by secreting cytokines and other ways.^{14,15} This motivated us to investigate the possibility and potential pathophysiological impact of macrophage-specific ADAR1 dysfunction in human cancers.

RESULTS

ADAR1 loss in macrophages potentially promotes antitumor immunity, as in cancer cells

To investigate a potential link between macrophage ADAR1 loss and antitumor immunity, we first interrogated its expression dynamics in normal and cancer-specific macrophages. We analyzed multiple single-cell RNA-sequencing (scRNA-seq) data sets of patients with human cancer to gauge the alteration of *ADAR* expression between TAMs and normal tissue-resident macrophages. Across four cancer types (ie, kidney,¹⁶ esophageal,¹⁷ gastric,¹⁸ and lung cancer),¹⁹ we observed a significant elevation of *ADAR* expression in TAMs (figure 1A–D). Expanding on this finding, we found that *ADAR* was ubiquitously expressed in monocytes and macrophages across almost all surveyed cancer types, according to a large-scale catalog, Tumor-Immune Single-Cell Hub 2 (TISCH 2)²⁰

(figure 1E). This finding is reminiscent of the reported amplification and overexpression of *ADAR* in numerous cancer types compared with normal tissues,^{2,21} suggesting that ADAR1 hyperactivation is employed as an immunosuppressive mechanism not only by cancer cells but by macrophages as well.

If this hypothesis holds, a therapeutic implication would be to inhibit ADAR1 activity in macrophages to reshape the tumor microenvironment towards a less immunosuppressive state. As demonstrated by Ishizuka *et al* in melanoma⁵ and by Mehdipour *et al* in colorectal cancer,⁶ the shared underlying mechanism of ADAR1-loss-mediated immune activation was the elevation of IFN signaling in cancer cells. We thus questioned whether suppressing TAM-specific ADAR1 would lead to the same IFN response. Using an RNA-seq data set derived from ADAR1-perturbed THP-1, a macrophage cell line, we examined the extent of IFN signaling boost based on a set of IFN response signature genes²² and found significant upregulation of many such genes (figure 1F). Thus, this result suggested that the monocyte/macrophage lineage possesses a robust ADAR1-IFN negative-feedback loop similar to cancer cells which when inhibited, could potentially promote antitumor immunity.

ADAR1 loss in macrophages combined with IFN- γ treatment results in tumor regression

To directly evaluate the effects of macrophage-specific ADAR1 loss on tumor growth, we first constructed *Adar*^{fl/fl} C57BL/6 mice, from which we then generated mice with a conditional knockout of the *Adar* gene in macrophages (*Adar*^{fl/fl}*Lyz2*^{cre}) (online supplemental figure S1A). We confirmed the macrophage-specific *Adar* loss by agarose gel electrophoresis analysis on the mouse genomic DNA (online supplemental figure S1B) and flow cytometry and western blot analysis on bone marrow-derived macrophages (BMDMs) (online supplemental figure S1C,D). To characterize the ADAR1-loss effects in different tumor contexts, we chose three major cancer types as disease models (ie, LLC for lung cancer, B16-F10 for melanoma, and MC38 for colon cancer). Given the critical role of IFN in triggering ADAR1-mediated immune response, we performed two sets of parallel experiments: compare the tumor growth between the two kinds of C57BL/6 mice (*Adar*^{fl/fl} vs *Adar*^{fl/fl}*Lyz2*^{cre}) with and without IFN- γ treatment after subcutaneous tumor cell inoculation (figure 2A). Strikingly, without IFN- γ treatment, there were no significant differences in tumor weight or size between the two groups; whereas with IFN- γ treatment, the size and weight of the tumors in the *Adar* knockout group were remarkably reduced (figure 2B–J, online supplemental figure S2). Notably, the IFN- γ treatment alone only weakly alleviated tumor growth in the control group. The consistent results across different experiments and disease models indicate that the combination of ADAR1 loss in macrophages and IFN- γ treatment can markedly inhibit tumor growth in diverse tumor contexts.

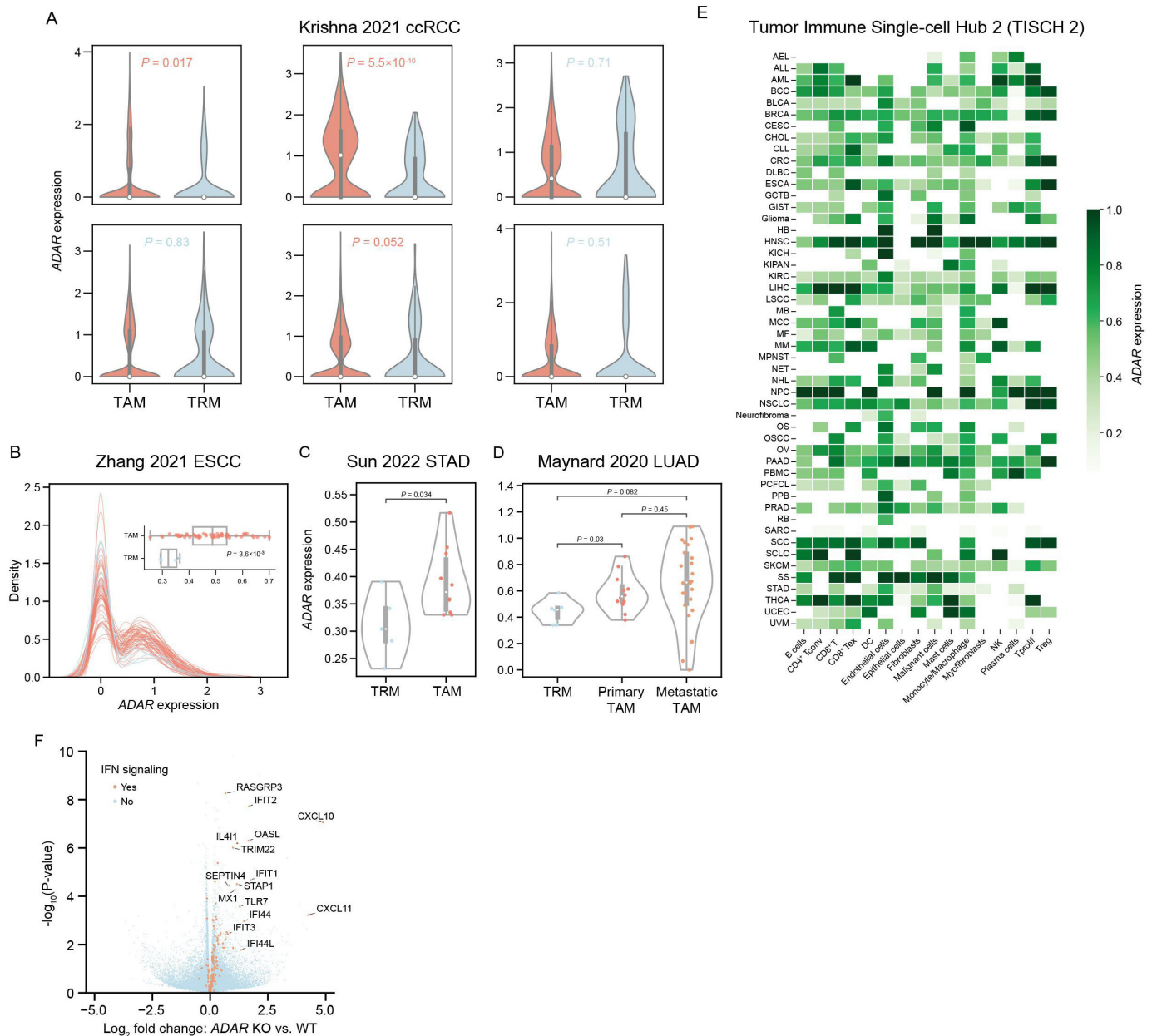


Figure 1 Functional effects of ADAR1 loss and ADAR1 expression in cancer cells and macrophages. (A) Violin plots showing the expression levels of *ADAR* in macrophages across six patients of clear cell renal cell carcinoma (ccRCC) with paired tumor versus normal samples from Krishna *et al.* (B) Density plots showing *ADAR* expression levels in TAMs and TRMs of 64 patients with esophageal cancer (ESCC) from Zhang *et al.* Box plots inside show sample-level average macrophage-specific *ADAR* expression levels between tumor and normal samples. (C) Violin plots showing sample-level average *ADAR* expression levels in macrophages across 14 patients with gastric cancer (STAD) with tumor versus normal samples from Sun *et al.* (D) Violin plots showing sample-level average *ADAR* expression levels in macrophages across 45 patients with lung adenocarcinoma (LUAD) with metastatic tumor, primary tumor, and normal samples from Maynard *et al.* (E) Heatmap showing the average cell-type-specific *ADAR* expression levels across cancer types based on single-cell RNA-sequencing data collected by Tumor-Immune Single-Cell Hub 2. (F) Volcano plot showing the differentially expressed genes in *ADAR*-deficient THP-1 cells. Highlighted and marked genes are members of the interferon signaling pathway. ADAR, adenosine deaminases acting on RNA; IFN, interferon; KO, knockout; TAMs, tumor-associated macrophages; TRM, tissue-resident macrophage; WT, wild type.

ADAR1 loss in macrophages combined with IFN- γ leads to differentiated regulation of key cytokines via upregulation of PKR/EIF2 α signaling

To elucidate the molecular mechanisms underlying the striking effects of the combination of ADAR1 loss in macrophages and IFN- γ treatment *in vivo*, we focused

on THP-1 as a representative cell model to study macrophage-related functions and mechanisms. We performed human cytokine arrays to detect differentially secreted cytokines, chemokines, and growth factors between the control and ADAR1-knockdown THP-1 cells (transfected with scrambled shRNA or shADAR1#1,

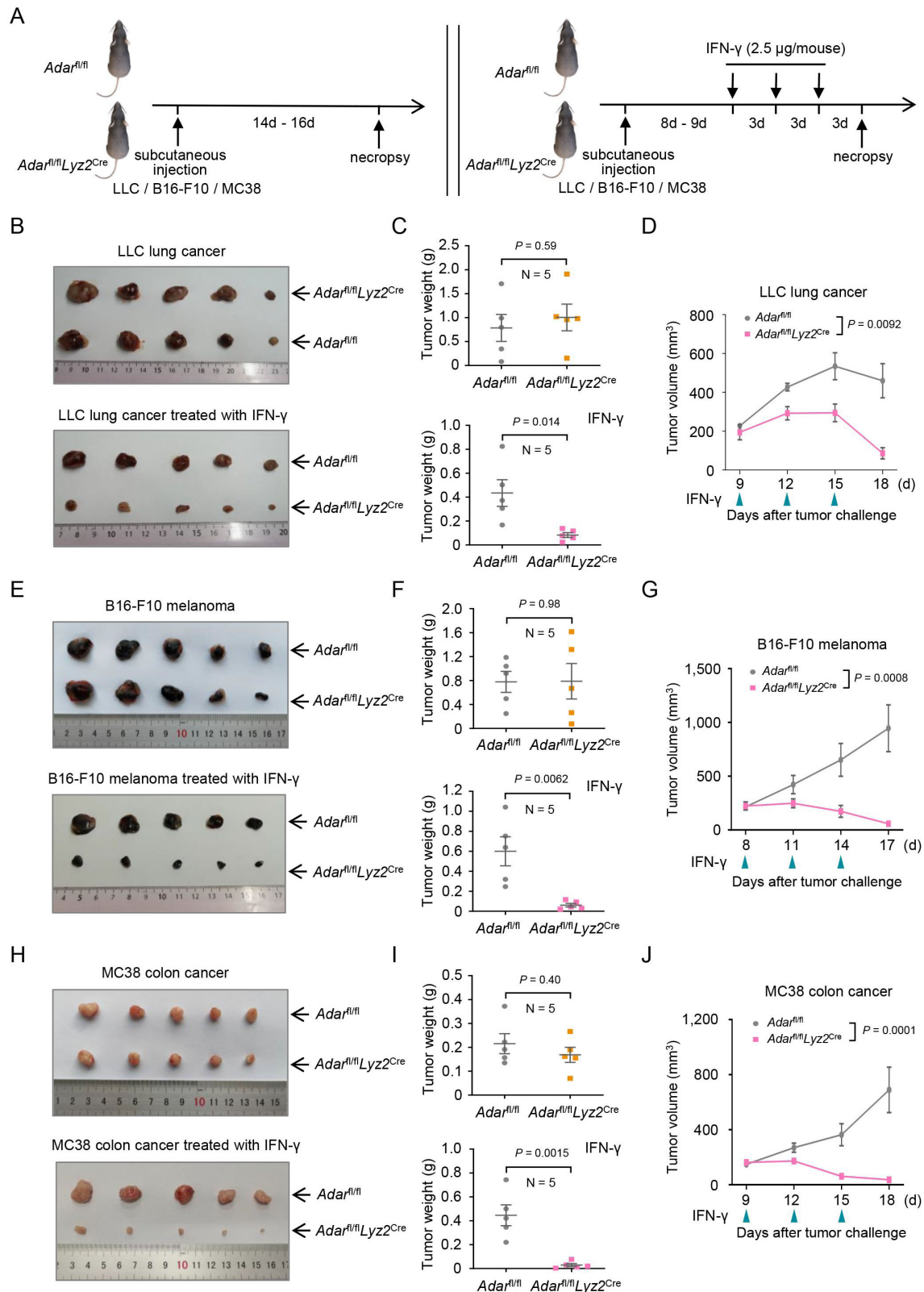


Figure 2 Effects of ADAR1 loss in macrophages with and without IFN- γ treatment on tumor growth. (A) Schematic diagram of the mouse models of three cancer types (lung, melanoma, and colon cancer) without and with IFN- γ treatment. (B, E, H) The images of tumors on the 14th-18th day without (top) and with IFN- γ treatment (bottom) in lung cancer (B) melanoma (E) and colon cancer (H). (C, F, I) Box plots showing the tumor weights without (top) and with IFN- γ treatment (bottom) in lung cancer (C) melanoma (F) and colon cancer (I). $N=5$ per group. Data are shown as mean \pm SEM, and p values are based on unpaired Student's t-test. (D, G, J) Tumor volume curves of the mouse models of lung cancer (D) melanoma (G) and colon cancer (J) with IFN- γ treatment. Tumor sizes were measured using calipers. Data are shown as mean \pm SEM, and p values are based on a two-way analysis of variance. ADAR, adenosine deaminases acting on RNA; IFN, interferon.

respectively, online supplemental figure 3A) treated with IFN- γ . We found that the secretion of CCL7, CCL20, CXCL11, GDF15, IL-18BP, PLAUR, and TIM-3 was significantly reduced in the ADAR1-knockdown cells, while IFN- γ secretion was increased (figure 3A,B). In parallel, we assessed differential cytokine secretion by THP-1 cells overexpressing ADAR1 (online supplemental figure S3B). When co-cultured with A549 cells, the secretion of CCL3/CCL4, CCL20, GDF15, PLAUR, and TIM-3 significantly increased on ADAR1 overexpression in THP-1 cells (figure 3C,D). Integrating the ADAR1 knockdown and overexpression analyses, we identified a set of key cytokines that were affected by ADAR1 in macrophages (figure 3E). Among them, CCL20 and GDF15 have been reported to promote vascular tube formation, while IFN- γ has an inhibitory effect^{11,23}; TIM-3 is a well-established immunosuppressive molecule,^{24–26} and interleukin (IL)-18BP acts as a secreted immune checkpoint to limit IL-18 immunotherapy efficacy in the tumor microenvironment.²⁷ These results suggest that macrophage ADAR1 loss and IFN- γ treatment may inhibit tumor growth by two mechanisms mediated by these key cytokines (1) suppress vessel formation by decreasing the secretion of CCL20 and GDF15 and increasing IFN- γ secretion, and (2) promote the abundance/function of CD8⁺ T cells by reducing the secretion of TIM-3 and IL-18BP.

To further investigate how these key cytokines are regulated by ADAR1 loss in macrophages, we first examined whether the differential cytokine secretion is due to the corresponding changes at the transcriptional level. We assessed the messenger RNA (mRNA) levels of *CCL20*, *GDF15*, *IFN-G*, *IL-18BP*, and *HAVCR2* (TIM-3) in different THP-1 cells (transfected with scrambled shRNA, shADAR1#1, or shADAR1#2, respectively) treated with IFN- γ . Intriguingly, we found that after knocking down ADAR1, the mRNA level of *IFN-G* exhibited a dramatic increase (>100-fold); however, the mRNA levels of *CCL20*, *GDF15*, and *HAVCR2* (in the shRNA#2 group) were also significantly increased, and the IL-18BP mRNA level showed limited variation (figure 3F). In parallel, we confirmed the same mRNA expression patterns of these four cytokines in BMDMs extracted from different groups of C57BL/6 mice (*Adar*^{fl/fl} vs *Adar*^{fl/fl}/*Lyz2*^{cre}) with IFN- γ treatment (figure 3G). These results suggest that on ADAR1 loss, increased secretion of IFN- γ is largely due to the dramatic transcriptional upregulation, but the reduced secretion of CCL20, GDF15, IL-18BP, and TIM-3 do not result from the reduced mRNA levels. We, therefore, speculated whether the downregulation of these cytokines was at the translational level.

Since ADAR1 is a dsRNA-binding protein that can reduce free dsRNA,^{28,29} a high level of dsRNAs resulting from ADAR1 knockdown could activate the expression of phosphorylated PKR, a global protein synthesis inhibitor and also a kinase of EIF2 α , thereby leading to the phosphorylation of EIF2 α and a shutdown of cellular and viral protein synthesis.^{30–33} We hypothesized that the reduced secretion of the above four key cytokines induced by

ADAR1 knockdown and IFN- γ treatment was due to the translational inhibition mediated by PKR/EIF2 α signaling. To test this hypothesis, we examined dsRNA amounts in different THP-1 cells (transfected with scrambled shRNA, shADAR1#1, or shADAR1#2, respectively) treated with IFN- γ using immunofluorescence. We found that the expression of dsRNA was significantly increased in the ADAR1 knockdown group, and as a negative control, the addition of RNase III³⁴ could specifically degrade the dsRNAs (figure 3H). We then used the dsRNA analog poly I:C⁷ for additional validation and observed upregulated protein expression of both p-PKR^{Thr446/Thr451} and p-EIF2 α ^{Ser51} after poly I:C treatment (figure 3I). After establishing a link between dsRNAs and phosphorylated PKR/EIF2 α , we next asked whether macrophage ADAR1 loss and IFN- γ treatment could cause the translational inhibition of CCL20, GDF15, IL-18BP, and TIM-3 through this mechanism. We measured the protein expression of p-PKR^{Thr446/Thr451}, PKR, p-EIF2 α ^{Ser51}, and EIF2 α in different THP-1 cells (transfected with scrambled shRNA, shADAR1#1, and shADAR1#2, respectively) treated with IFN- γ . Indeed, the protein expression of p-PKR^{Thr446/Thr451} and p-EIF2 α ^{Ser51} was significantly increased with ADAR1 knockdown (figure 3J). We then used an inhibitor of phosphorylated PKR, 2-aminopurine (2-AP),^{35–37} which inhibited the protein expression of phosphorylated PKR at Thr446 and Thr451, to the different THP-1 cells after IFN- γ treatment, and observed a reduced protein expression of p-EIF2 α ^{Ser51} accordingly (figure 3K). To further confirm the effects on our targeted cytokines, using ELISA, we verified the reduced secretion of CCL20, GDF15, IL-18BP, and TIM-3 in the conditioned medium of macrophages from C57BL/6 mice (*Adar*^{fl/fl}/*Lyz2*^{cre}) treated with IFN- γ (figure 3L). Furthermore, the secretion of these cytokines could be significantly prompted by the addition of 2-AP (figure 3L). After IFN- γ treatment, ADAR1-knockout THP-1 cells showed a dramatic increase in *IFN-G* mRNA, but the magnitude of IFN- γ secretion increase was much lower (figure 3B,F). IFN- γ secretion increased more after PKR activity was inhibited by 2-AP (online supplemental figure S3C), indicating that activated PKR still inhibited IFN- γ translation to some extent. Thus, although activated PKR inhibits IFN- γ translation, ADAR1-deficient macrophages stimulated by IFN- γ produce a much larger amount of *IFN-G* mRNA to compensate for this effect. As a result, the net IFN- γ secretion was still increased.

Recent studies have shown that IL-18 is an activator of cytotoxic T lymphocytes (CTLs) and enhances antitumor immunity,^{27,38} and in the tumor microenvironment, IL-18BP acts as an immune checkpoint for IL-18 immunotherapy efficacy.²⁷ Given the relationship between IL-18BP and IL-18, we also examined the level of IL-18 in the above experiments. Intriguingly, unlike CCL20 and GDF15, IL-18 showed an increase at the mRNA, protein, and secretion levels on ADAR1 loss (figure 3F, G and L, online supplemental figure S4A). We, therefore, sought

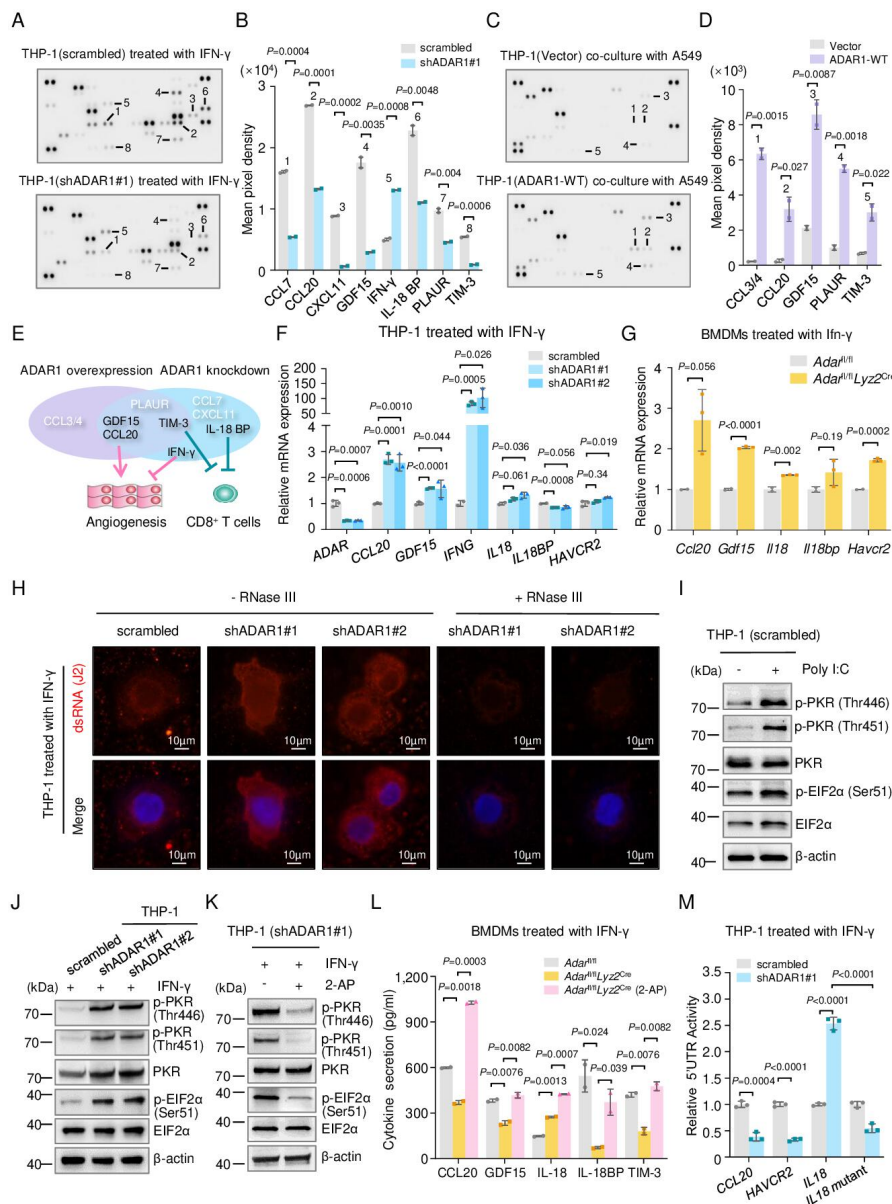


Figure 3 ADAR1 loss in macrophage with IFN- γ treatment affects the secretion of key cytokines through PKR/EIF2 α signaling. (A, C) Human XL cytokine arrays for detecting differential factors between THP-1 cells with scrambled shRNA and shADAR1#1 under the treatment of IFN- γ (A) and between THP-1 cells with empty vector and WT *ADAR*, co-cultured with A549 (C). (B, D) Bar plots showing the expression levels of differential factors on ADAR1 knockdown (B) and ADAR1 overexpression (D). (E) Venn gram showing key cytokines identified by ADAR1 knockdown and overexpression experiments and their potential effects on the tumor microenvironment. (F) RT-qPCR-based mRNA expression levels of *ADAR*, *CCL20*, *GDF15*, *IFN-G*, *IL-18*, *IL-18BP*, and *HAVCR2* in different THP-1 cells (transfected with scrambled shRNA, shADAR1#1 or shADAR1#2) with IFN- γ treatment. β -actin was used as an internal control. (G) RT-qPCR-based mRNA expression levels of *Ccl20*, *Gdf15*, *Il-18*, *Il-18bp*, and *Havcr2* in BMDMs from C57BL/6 mice (*Ada*^{fl/fl} and *Ada*^{fl/fl}*Lyz2*^{Cre}) treated with IFN- γ . *Gapdh* was used as an internal control. (H) Immunofluorescent staining for anti-dsRNA (J2) in THP-1 cells treated with IFN- γ . RNase III treatment was used as the negative control for the dsRNA signal. Scale bars, 10 μ m. (I) Western blot showing the protein expression of p-PKR^{Thr446/Thr451}, PKR, p-EIF2 α ^{Ser51}, and EIF2 α protein expression in THP-1 cells transfected with scrambled shRNAs and treated with poly I:C (1 μ g/mL). (J) Western blot showing the protein expression of p-PKR^{Thr446/Thr451}, PKR, p-EIF2 α ^{Ser51}, and EIF2 α expression in THP-1 cells (transfected with scrambled, shADAR1#1, or shADAR1#2) with IFN- γ treatment. (K) Western blot showing the protein expression levels of p-PKR^{Thr446/Thr451}, PKR, p-EIF2 α ^{Ser51}, and EIF2 α protein expression in THP-1(shADAR1#1) cells with IFN- γ after pretreatment with or without 2-AP. (L) ELISA quantitative measurement of Ccl20, Gdf15, IL-18, IL-18bp, and Tim-3 from conditioned media of different BMDMs (*Ada*^{fl/fl}, *Ada*^{fl/fl}*Lyz2*^{Cre}, and *Ada*^{fl/fl}*Lyz2*^{Cre} with 2-AP) treated with IFN- γ . (M) Dual luciferase reporter assays for the 5'UTR activities of *CCL20*, *HAVCR2*, *IL-18*, and *IL-18-Mutant*. Data are normalized to renilla luciferase. (B, D, F, G, L, and M) Data are shown as mean \pm SD, and p values are based on unpaired Student's t-test. (I, J and K) β -actin was used as the loading control. ADAR, adenosine deaminases acting on RNA; BMDMs, bone marrow-derived macrophages; dsRNAs, double-stranded RNAs; IFN, interferon; IL, interleukin; mRNA, messenger RNA; RT-qPCR, reverse transcription-quantitative polymerase chain reaction; WT, wild type; 2-AP, 2-aminopurine.

to elucidate how the IL-18 secretion was not affected by PKR/EIF2 α -mediated translational inhibition. Under cellular stress, p-EIF2 α suppresses the global translation, but a few genes can escape this effect due to the presence of upstream ORFs (uORFs) in their 5'UTRs region, such as *ATF4*.³⁹ Indeed, we found that *IL-18* contains a uORF in the 5'UTR but not *CCL20* or *HAVCR2*. To test our hypothesis that IL-18 was allowed to be translated by p-EIF2 α due to the uORF, we constructed 5'UTR dual-luciferase reporter plasmids for *CCL20*, *HAVCR2*, and *IL-18* and examined their activities in different THP-1 cells. We found that the 5'UTR activity of *CCL20* and *HAVCR2* in THP-1 cells with ADAR1 knockdown after IFN- γ treatment was significantly lower than that in the control cells, whereas the 5'UTR activity of *IL-18* was significantly increased (figure 3M). To further confirm our hypothesis, we introduced a mutation to the uORF to destroy its uORF motif. We found that the luciferase reporter activity diminished significantly in the ADAR1-knockdown THP-1 cells with the *IL-18* uORF point mutation (figure 3M). To explore the underlying mechanisms, we performed a Kyoto Encyclopedia of Genes and Genomes (KEGG) pathway analysis of differentially expressed genes identified from the RNA-seq data from THP-1 cells treated with IFN- γ (scrambled vs shADAR1#1) and observed an activation of the nuclear factor kappa-B (NF- κ B) pathway on ADAR1 loss (online supplemental figure S4B). Additionally, we found an increased mRNA expression of *STAT4* (online supplemental figure S4C). Thus, the transcriptional upregulation induced by IFN- γ may be due to the increase in IL-18 secretion, as well as downstream transcriptional regulation mediated by NF- κ B and STAT4.

Taken together, our results indicate that with IFN- γ treatment, ADAR1-deficient macrophages accumulate free dsRNA that activates PKR/EIF2 α signaling and results in the translational inhibition of CCL20, GDF15, TIM-3, and IL-18BP, whereas IFN- γ secretion increases due to its extremely high mRNA upregulation and IL-18 secretion is also increased because its 5'UTR uORF allows escaping from global protein translational inhibition.

ADAR1 loss in macrophages combined with IFN- γ treatment decreases angiogenesis

Given the established role of CCL20 and GDF15 in promoting vessel formation and the opposite role of IFN- γ (figure 3E), we questioned whether macrophage ADAR1 deletion and IFN- γ treatment could inhibit tumor growth in vivo by affecting vessel formation. We first performed immunohistochemical staining on tumor sections of LLC from different groups of mice (*Adar*^{fl/fl} vs *Adar*^{fl/fl}*Lyz2*^{cre}) and measured CD31, a vascular hallmark. Without IFN- γ treatment, there were no significant differences in blood vessels of varied sizes between the ADAR1 knockout and control groups (figure 4A,B). In contrast, with IFN- γ treatment, the *Adar* knockout group showed much fewer large blood vessels (figure 4C,D), indicating that ADAR1 knockout in macrophages combined with IFN- γ treatment inhibits the formation of tumor

blood vessels. Next, we extracted macrophages from mice (*Adar*^{fl/fl} vs *Adar*^{fl/fl}*Lyz2*^{cre}), collected conditioned media after IFN- γ treatment, and used them for tube-forming experiments in mouse lymphoid endothelial cell line SVEC4-10. We found that *Adar*-knockout macrophages under IFN- γ treatment significantly inhibited tube formation in SVEC4-10 cells in terms of vessel area, the total number of junctions, and total vessel length (figure 4E,F). In parallel, we collected three groups of conditioned media from THP-1 cells (transfected with scrambled shRNA, shADAR1#1, or shADAR1#2, respectively) treated with IFN- γ for tube formation experiments in human umbilical vein endothelial cell line HUVEC. Consistently, we observed that ADAR1-knockdown THP-1 cells significantly inhibited tube formation in HUVEC cells (figure 4G,H). In addition, we tested the effects of conditioned media from three THP-1 cells (with vector, ADAR1-WT or ADAR1-E912A) on the tube-forming ability of HUVEC cells. We observed that exogenous overexpression of ADAR1-WT in THP-1 cells significantly promoted tube formation. ADAR1-E912A (the mutant with an abolished RNA editing activity) also showed a similar capacity to promote tube formation (figure 4I,J), suggesting that ADAR1 improves vascular tube formation independent of its RNA-editing activity.

To confirm that CCL20, GDF15, and IFN- γ were the key downstream effectors of ADAR1, we performed a tube formation experiment in SVEC4-10 cells treated with conditioned media from *Adar*^{fl/fl} versus *Adar*^{fl/fl}*Lyz2*^{cre} BMDMs and CCL20, GDF15, or IFN- γ (figure 5A). We observed that IFN- γ significantly inhibited tube formation, while both CCL20 and GDF15 significantly promoted tube formation (figure 5B,C). Moreover, when we pretreated supernatants from mouse macrophages (*Adar*^{fl/fl}*Lyz2*^{cre}) with 2-AP and then added IFN- γ , the decreased tube-forming ability of SVEC4-10 cells was restored (figure 5D,E). In a similar experiment using supernatants of THP-1 cells, 2-AP also recovered the reduced tube-forming ability of HUVEC cells (figure 5F,G). Collectively, these results indicate that IFN- γ -treated ADAR1-deficient macrophages inhibit angiogenesis through decreased CCL20 and GDF15 secretion and increased IFN- γ secretion.

ADAR1 loss in macrophages combined with IFN- γ treatment induces CD8⁺ T cell-dependent antitumor immunity

Given that TIM-3 and IL-18BP are established immunosuppressive molecules (figure 3E), we next aimed to understand how IFN- γ treatment of ADAR1-deficient macrophages affects CD8⁺ T-cell function. We first performed immunofluorescent and immunohistochemical staining of CD8a in mouse tumor tissues to assess the amount of CTLs. We found no significant difference in the tumor tissues between different mouse groups (*Adar*^{fl/fl} vs *Adar*^{fl/fl}*Lyz2*^{cre}) with and without IFN- γ treatment (figure 6A,B, online supplemental figure S5A). The flow cytometry analysis on extracted CD8⁺ T cells from tumor tissues of LLC C57BL/6 mice also showed no difference in CD8⁺ T-cell numbers between the two mouse groups

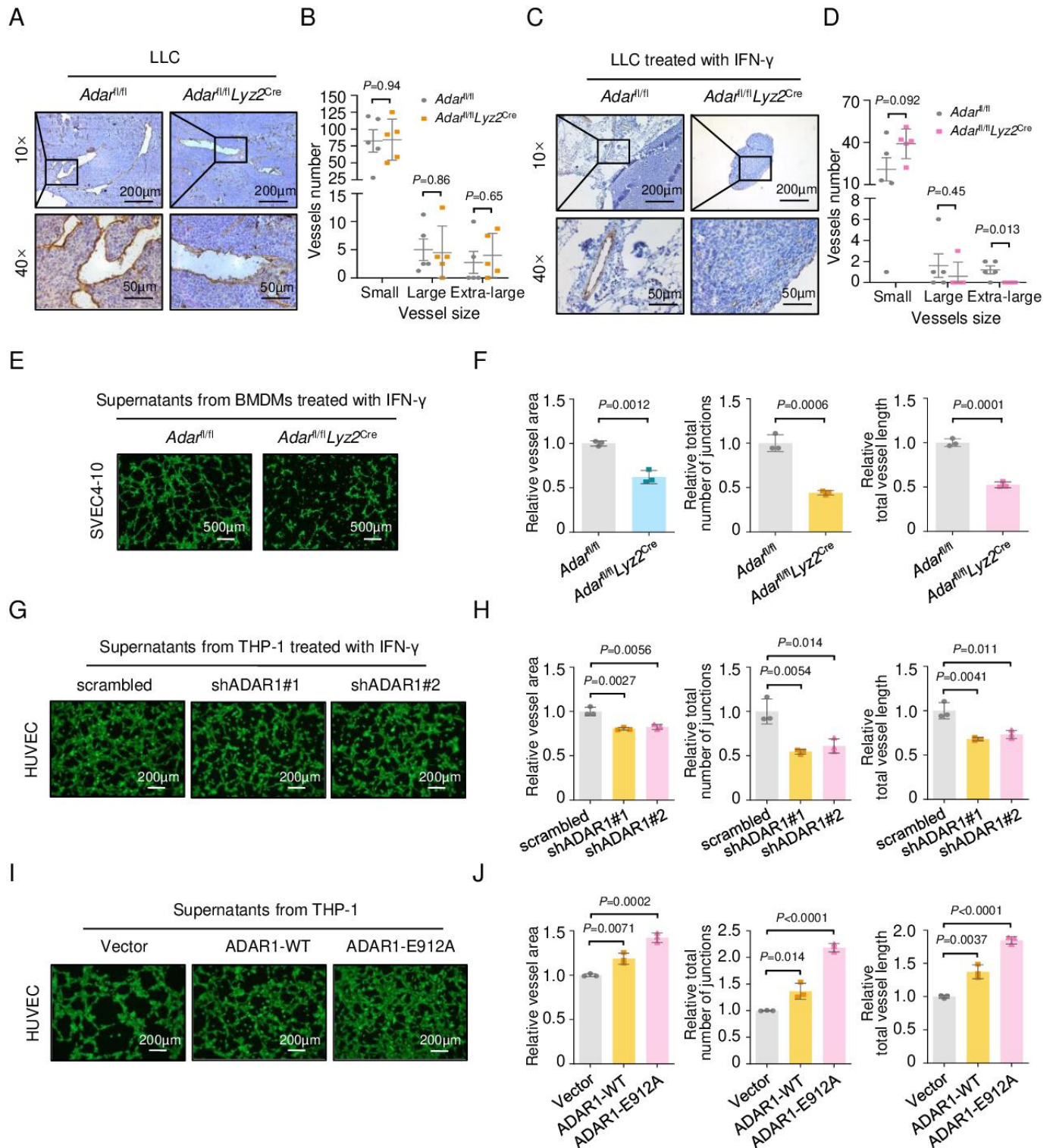


Figure 4 The effect of macrophage ADAR1 loss and IFN- γ treatment on angiogenesis. (A, C) Representative images of the paraffin-embedded LLC tumor tissue sections immunohistochemically stained with CD31 without (A) and with (C) IFN- γ treatment. Scale bar, 200 μ m. (B, D) The blood vessel numbers of different sizes in the two mouse models (*Adar*^{fl/fl}, *Adar*^{fl/fl}*Lyz2*^{Cre}) without (B) and with IFN- γ treatment (D). Data are shown as mean \pm SEM. (E) Tube formation of SVEC4-10 cells treated with different conditioned media from BMDMs (*Adar*^{fl/fl}, *Adar*^{fl/fl}*Lyz2*^{Cre}) and IFN- γ . Scale bar, 500 μ m. (F) Bar plots showing relative vessel area, the total number of junctions, and the vessel length for SVEC4-10 cell tube formation. (G, I) Tube formation of HUVEC cells treated with different conditioned media from THP-1 cells (transfected with scrambled shRNA, shADAR1#1, and shADAR1#2) and IFN- γ (G) and with *ADAR* (empty vector, *ADAR*-WT, and *ADAR*-E912A) (I). Scale bar, 200 μ m. (H, J) Bar plots showing relative vessel area, the total number of junctions, and the vessel length for HUVEC cells with different treatments of G (H) and I (J). (F, H, and J) Data are shown as mean \pm SD. (B, D, F, H, and J) P values are based on unpaired Student's t-test. ADAR, adenosine deaminases acting on RNA; BMDMs, bone marrow-derived macrophages; IFN, interferon; WT, wild type.

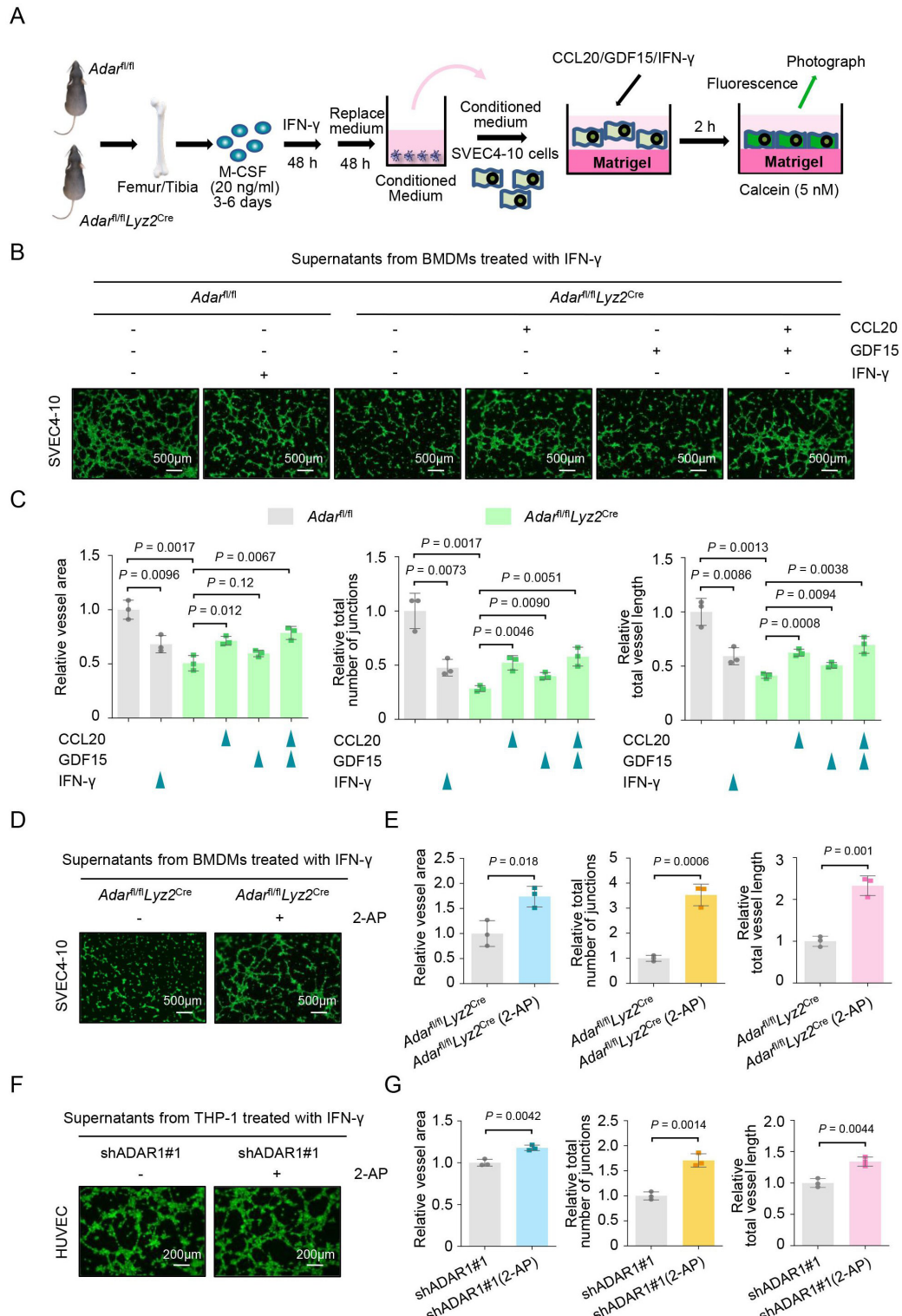


Figure 5 The effect of ADAR1 loss and key cytokines on tube formation. (A) Schematic diagram of tube formation experiment of SVEC4-10 cells. (B) Tube formation of SVEC4-10 cells treated with conditioned media from BMDMs (*Adar^{fl/fl}* vs *Adar^{fl/fl}Lyz2^{Cre}*) and CCL20, GDF15, or IFN- γ . Scale bar, 500 μ m. (C) Bar plots showing relative vessel area, the total number of junctions, and the vessel length for SVEC4-10 tube formation. (D) Tube formation of SVEC4-10 cells treated with conditioned media from BMDMs (*Adar^{fl/fl}Lyz2^{Cre}*) and IFN- γ after pretreatment with or without 2-AP (5 mM). Scale bar, 500 μ m. (E) Bar plots showing relative vessel area, the total number of junctions, and vessel length for SVEC4-10 tube formation. (F) Tube formation of HUVEC cells treated with conditioned media from THP-1 cells (transfected with shADAR1#1) and IFN- γ after pretreatment with or without 2-AP (5 mM). Scale bar, 200 μ m. (G) Bar plots showing relative vessel area, the total number of junctions, and the vessel length for HUVEC tube formation. (C, E, and G) P values are based on unpaired Student's t-test. Data are presented as mean \pm SD. ADAR, adenosine deaminases acting on RNA; BMDMs, bone marrow-derived macrophages; IFN, interferon; 2-AP, 2-aminopurine.

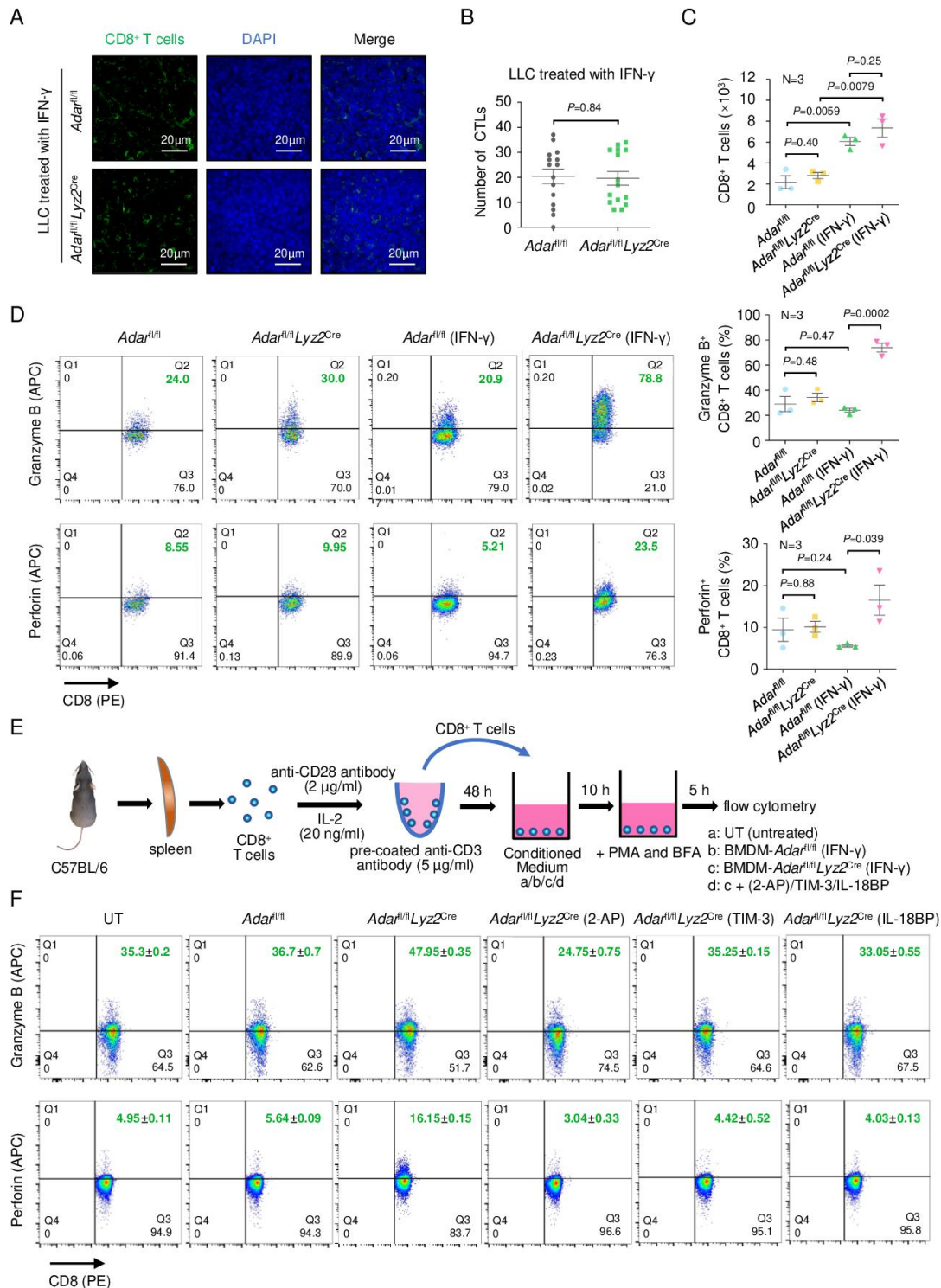


Figure 6 The combination effect of macrophage ADAR1 loss and IFN- γ treatment on CD8⁺ T cells. (A) Immunofluorescence staining with CD8 α antibody of the LLC xenograft tumors from C57BL/6 mice, representative cases are shown. Scale bar, 20 μ m. (B) Plot showing the distribution of the number of CTLs quantified by immunofluorescence staining. (C) Plot showing the number of CD8⁺ T cells in tumors from different mouse groups, quantified by flow cytometry. (D) Flow cytometry analysis of the expression of granzyme B and perforin in CD8⁺ T cells from xenograft tumors of different mouse groups. N=3. Plots showing the percentage of granzyme B⁺ or perforin⁺ CD8⁺ T cells in tumors from different mouse groups. (E) Schematic diagram of the conditioned medium culture of CD8⁺ T cells. (F) Flow cytometry analysis of the expression of granzyme B and perforin in CD8⁺ T cells treated with conditioned media from different BMDMs (Adar^{fl/fl} and Adar^{fl/fl}Lyz2^{Cre}) and 2-AP, TIM-3, or IL-18BP. (B–D) Data are shown as mean \pm SEM. P values are based on unpaired Student's t-test. ADAR, adenosine deaminases acting on RNA; APC, allophycocyanin; BFA, brefeldin A; BMDM, bone marrow-derived macrophage; CTLs, cytotoxic T lymphocytes; DAPI, 4'6-diamidino-2-phenylindole; IFN, interferon; IL, interleukin; PMA, Phorbol 12-myristate 13-acetate; UT, untreated; 2-AP, 2-aminopurine.

(figure 6C, online supplemental figure S5B). We next assessed the cytotoxic activity of CD8⁺ T cells using granzyme B and perforin and found that infiltrating CD8⁺ T cells in *Adar*-knockout mice had significantly higher cytotoxic activity (figure 6D, online supplemental figure S5B).

To confirm the effect of macrophage ADAR1 loss on the cytotoxic activity of CD8⁺ T cells, we collected macrophage-conditioned media from different mouse groups (*Adar*^{fl/fl} vs *Adar*^{fl/fl}*Lyz2*^{Cre}) treated with IFN-γ and examined granzyme B and perforin levels using flow cytometry (figure 6E). Consistently, we found that the conditioned media from *Adar*^{fl/fl}*Lyz2*^{Cre} macrophages significantly increased the cytotoxic activity of CD8⁺ T cells, and this was reversed by adding 2-AP, TIM-3, or IL-18BP (figure 6F, online supplemental figures S6 and S7). In addition, we found that macrophage *Adar*-knockout did not affect the chemotactic ability of CD8⁺ T cells (online supplemental figure S6C–F). Overall, these results demonstrate that

ADAR1 loss in macrophages combined with IFN-γ treatment promotes the cytotoxic function of CD8⁺ T cells by increasing the release of granzyme B and perforin, thereby contributing to a tumor microenvironment that can kill tumor cells more efficiently.

The combination of ADAR1-deficient macrophages and IFN-γ treatment is a potential therapeutic approach

Finally, to explore the translational potential of our findings, given the recent interest in engineered macrophages for cancer immunotherapy, we sought to test whether ADAR1-deficient macrophages could be used as cancer therapeutics. We extracted BMDMs from mice (*Adar*^{fl/fl} vs *Adar*^{fl/fl}*Lyz2*^{Cre}) and injected ADAR1-deficient macrophages into the LLC-tumor-bearing mice through the tail vein. Next, we treated these mice with IFN-γ at different time points (figure 7A). Strikingly, injection of knockout-ADAR1 macrophages combined with IFN-γ remarkably

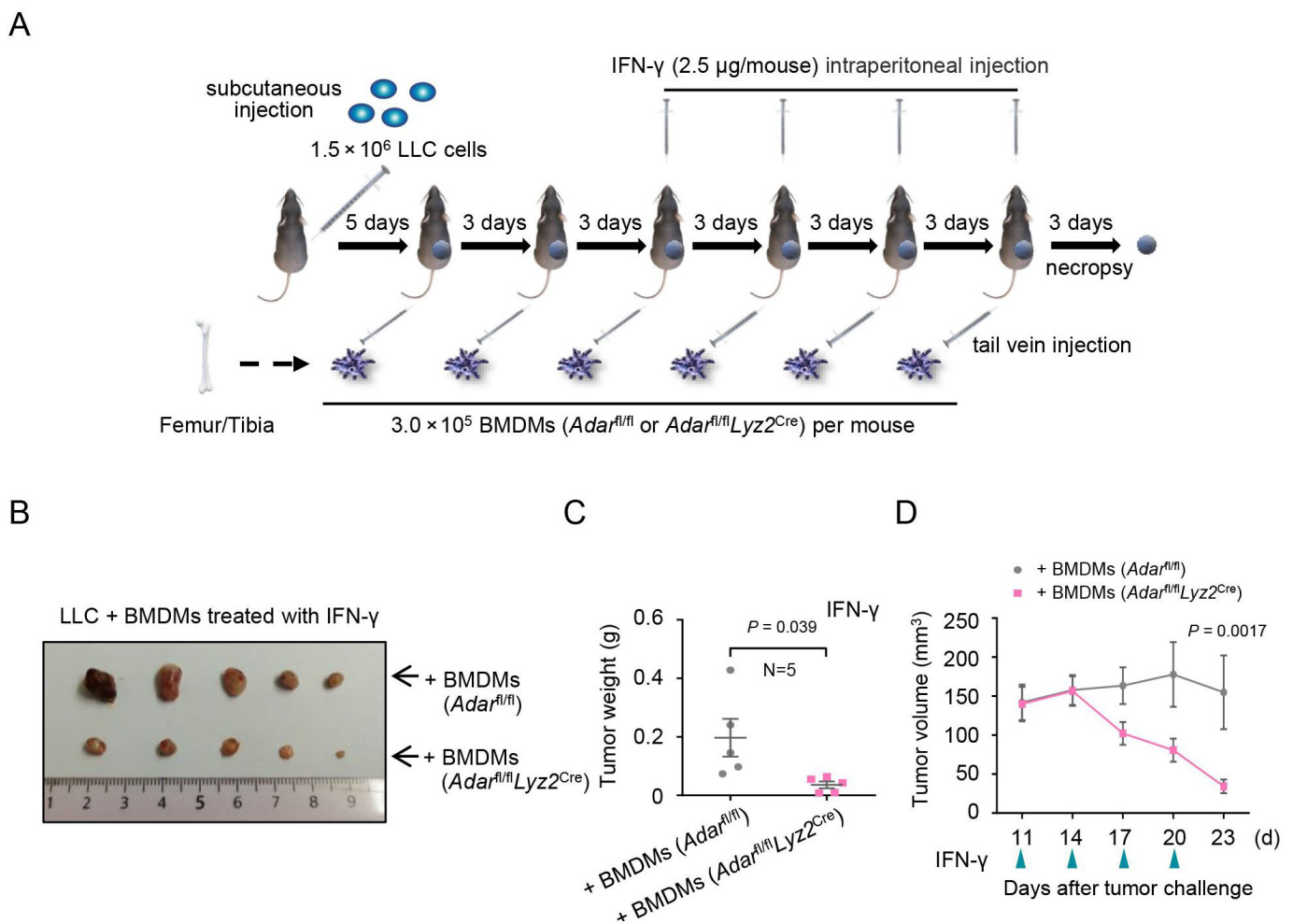


Figure 7 The combination effect of ADAR1-deficiency macrophages and IFN-γ treatment on tumor growth. (A) Schematic diagram of the LLC xenograft mouse models treated with engineered ADAR1-deficient macrophages. BMDMs from C57BL/6 mice (*Adar*^{fl/fl} and *Adar*^{fl/fl}*Lyz2*^{Cre}) were injected into the tail vein, combined with IFN-γ. Necropsies were performed 23 days after the injection of the LLC cells. (B) The images of tumors on the 23rd day (C) plot showing the weight of tumors. *N* = 5. *P* value is based on unpaired Student's *t*-test. (D) The tumor volume curves during the treatment course. *P* value is based on a two-way analysis of variance with Sidak's multiple comparison test. Tumor sizes were measured using calipers. *N* = 5. (C, D) Data are shown as mean ± SEM. ADAR, adenosine deaminases acting on RNA; BMDM, bone marrow-derived macrophage; IFN, interferon.

inhibited tumor growth and led to tumor regression (figure 7B–D). Importantly, we did not observe obvious side effects in the mouse model. These results highlight the potential of engineered ADAR1-deficient macrophages and IFN- γ as an effective combination therapy to treat tumors.

DISCUSSION

Here we show that ADAR1 loss in macrophages combined with IFN- γ treatment provides a stimulus that reprograms the tumor microenvironment and inhibits the growth of diverse tumors. Since no significant antitumor effect was detected when macrophages were only subjected to ADAR1 loss, the phenomenon we report is a synergistic effect, rather than a simple additive effect. We further demonstrate that ADAR1-deficient macrophages can serve as a therapeutic in combination with IFN- γ to inhibit tumors effectively. Mechanistically, the combination of ADAR1 loss in macrophages and IFN- γ leads to the differential secretion of key cytokines: decreased CCL20, GDF15, IL-18BP, and TIM-3 through PKR/EIF2 α -mediated translational inhibition; and increased IFN- γ due to strong transcriptional upregulation and increased IL-18 due to the presence of a uORF in the 5'UTR of its gene. Consequently, suppression of CCL20 and GDF15, as well as increased IFN- γ reduce tumor vascularization, while the reduction of IL-18BP and TIM-3 and increase in IL-18 promote the cytotoxic function of CD8⁺ T cells. These effects collectively reprogram the tumor microenvironment, turning a “cold tumor” into a “hot tumor” (figure 8). Our study provides a more comprehensive view of how ADAR1-mediated signaling can affect the whole tumor ecosystem beyond cancer cells.

Our study also provides novel insights into an emerging immunotherapy target, TIM-3. A growing body of literature suggests that high expression of TIM-3 on CD8⁺ T cells is the main marker of T-cell exhaustion, and the therapeutic blockade of TIM-3 is being investigated in multiple human malignancies.³⁸ As a receptor, TIM-3 is not only expressed on the surface of CD8⁺ T cells, which functions as an immunosuppressive checkpoint,⁴⁰ but also on various types of immune cells, such as macrophages and dendritic cells.^{24, 38} A recent study reports that the loss of TIM-3 on the surface of dendritic cells promotes antitumor immunity.³⁸ Besides being a surface receptor, TIM-3 also has a soluble form in plasma.^{41, 42} Although the expression of the plasmid encoding soluble TIM-3 in vivo significantly promotes tumor growth by damaging the antitumor immunity mediated by T cells,⁴³ the function of secreted TIM-3 in the tumor microenvironment is not clear. Here we demonstrate that reduced secretory TIM-3 can promote the cytotoxic function of CD8⁺ T cells. Thus, our study suggests a conceptually novel role of TIM-3, contributing to a deeper understanding of TIM-3 as an immunosuppressive checkpoint, similar to secreted IL-18BP.²⁷ Thus, secretory TIM-3 may be a biomarker to assess antitumor immunity.

The most exciting part of our study is the synergetic effect of ADAR1-deficient macrophages and IFN- γ in tumor elimination. IFN- γ exerts antitumor immunity by enhancing the function of tumor-infiltrating immune cells such as TH1 cells, CTLs, and macrophages, inhibiting the function of regulatory T cells (Tregs) and regulating the function of stromal cells.⁴⁴ IFN- γ treatment has been approved by the US Food and Drug Administration to cure chronic granuloma and osteoporosis.^{45, 46} With ADAR1-deficient macrophages, IFN- γ treatment cannot only slow tumor growth but even lead to tumor shrinkage. As an initial attempt to test the translational potential of our findings, we injected ADAR1-knockout macrophages into mice combined with IFN- γ and observed remarkable tumor-killing effects. Importantly, there were no serious side effects in the mice, suggesting a viable treatment strategy. Several therapeutic strategies have been proposed based on targeting ADAR1 in tumor cells in combination with other therapies such as radiotherapy, chemotherapy, and epigenetic therapy.^{5, 6} However, due to tumor heterogeneity and severe side effects, it would be quite challenging to implement such strategies for the majority of patients. Our approach is based on ADAR1-deficient macrophages, representing a fundamentally distinct strategy for targeting ADAR1. Since cancer development is usually accompanied by a large amount of infiltrated macrophages⁴⁷ that reshape the tumor microenvironment to support tumor progression, our approach may have some unique advantages.

Given that our study serves as an initial endeavor, it is imperative to undertake further endeavors to thoroughly assess the viability of this strategy. This entails the following endeavors: (1) Expanding our investigations to encompass a broader range of tumor types and incorporating spontaneous tumor models, along with embracing a diverse spectrum of animal models such as canines and primates. (2) Fine-tuning the dosages of IFN- γ , as well as meticulously optimizing the parameters related to the source, quantity, and injection frequency of macrophages. (3) Exploring alternative therapeutic avenues by delving into the realm of other pivotal cytokines, thereby broadening our understanding and options for treatment. This multifaceted approach will be crucial in advancing our comprehension and clinical application of this strategy.

Online methods scRNA-seq data analysis

We analyzed data from four human patient cohorts where tumor samples and paired or unpaired normal tissues were collected for single-cell gene expression profiling. For Krishna *et al*,¹⁶ we downloaded a Seurat object that contains raw Unique Molecular Identifiers (UMI) counts and cell type annotations from Sequence Read Archive (SRA, <https://www.ncbi.nlm.nih.gov/sra>) under accession number SRZ190804. For Zhang *et al*,¹⁷ we obtained a myeloid-specific UMI count matrix from the Gene Expression Omnibus (GEO, <https://www.ncbi.nlm.nih.gov/geo/>) under accession number GSE160269. For Sun *et al*, 2020,¹⁸ we downloaded

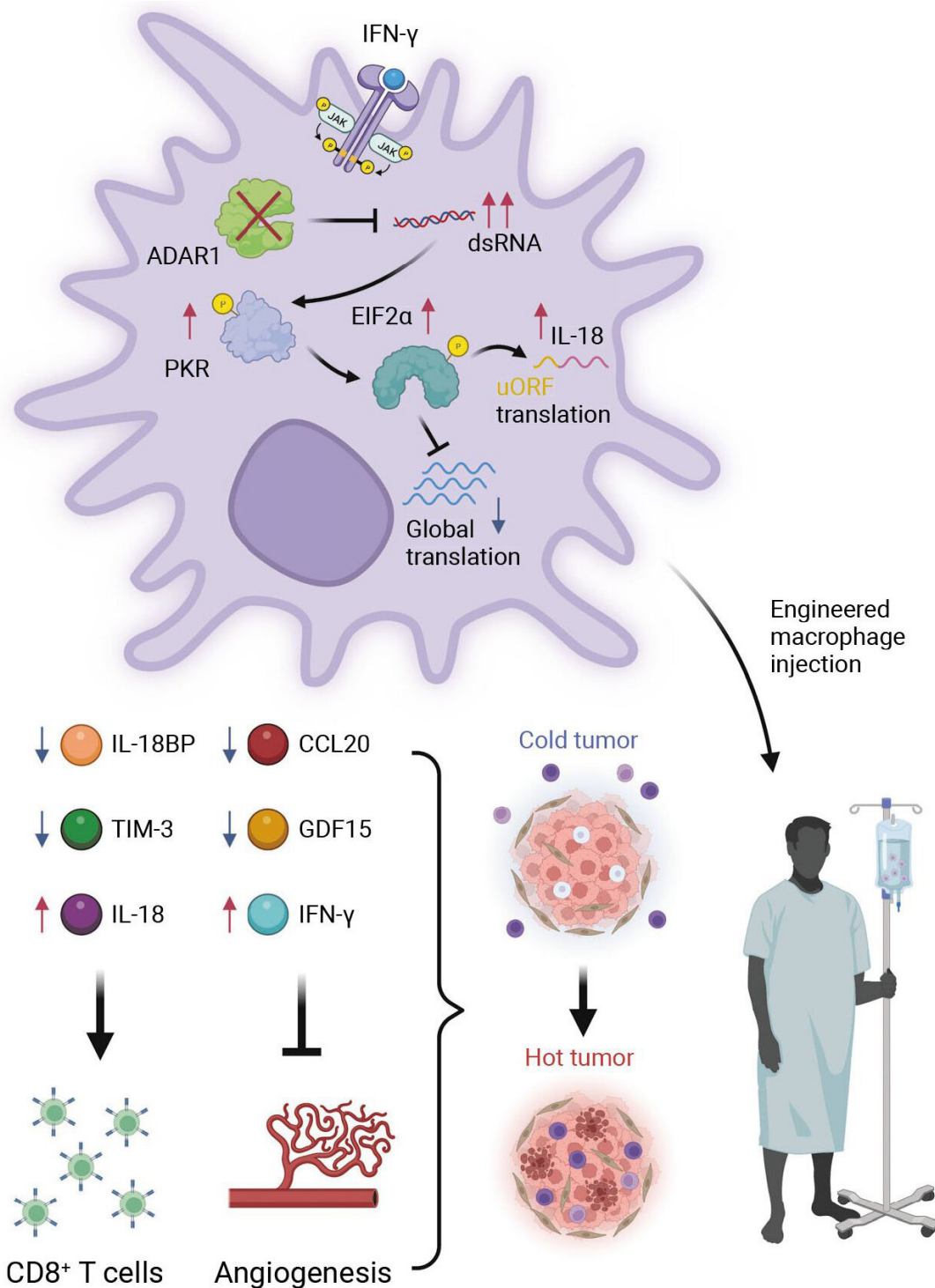


Figure 8 Schematic summary of this study. ADAR1-deficient macrophages combined with IFN- γ treatment reprogram the tumor microenvironment by two mechanisms: (1) inhibit angiogenesis by decreased secretion of GDF15 and CCL20 and increased secretion of IFN- γ , and (2) activate CD8 $^+$ T cells by decreased secretion of TIM-3 and IL-18BP and increased secretion of IL-18. These effects collectively convert a “cold tumor” into a “hot tumor.” Combined treatment with ADAR1-deficient macrophages and IFN- γ may represent an effective therapeutic approach. dsRNA, double-stranded RNA; IFN, interferon; IL, interleukin; uORF, upstream Open Reading Frame.

log₂-transformed normalized UMI counts from the Open Archive for Miscellaneous Data (OMIX, <https://ngdc.cncb.ac.cn/omix/>) under accession number OMIX001073. For Maynard *et al.*¹⁹ a Seurat object of immune cells was downloaded from GitHub ([https://](https://github.com/czbiohub/scell_lung_adenocarcinoma)

github.com/czbiohub/scell_lung_adenocarcinoma). Myeloid cells were subsequently extracted for expression analyses. No preprocessing or quality control was further applied beyond what was already conducted by the original studies. To ensure fair comparisons

and robust testing of differential *ADAR* expressions, we focused on sample-level pseudo-bulk comparisons, except for Krishna *et al*, 2021 where all six patients had paired tumor and normal samples, so the comparison was limited within each patient. For a comprehensive survey of *ADAR* expressions across cell types in cancer tissues, we queried its expression in TISCH 2 (<https://tisch.comp-genomics.org/>),²⁰ respectively, two databases that host the most complete catalogs of scRNA-seq profiles to our knowledge.

Bulk RNA-seq data analysis

We analyzed an RNA-seq data set of a human leukemia monocytic cell line THP-1 with CRISPR/cas9-based knockout of *ADAR*. Gene count matrices were downloaded from GEO under the accession number GSE176012. The differential gene expression analysis was conducted using DESeq2 (V.1.34.0)⁴⁸ with log₂-fold changes and adjusted *p* values as output.

Cell culture

THP-1, LLC, HEK-293, A549, MC38, and B16-F10 cells were obtained from the National Collection of Authenticated Cell Cultures and Cell Bank, Chinese Academy of Sciences (Shanghai, China), and American Type Culture Collection (ATCC). HUVEC and SVEC4-10 cells were obtained from Procell Life Science&Technology. All cell lines were confirmed by short tandem repeat analyses and were *Mycoplasma* negative. LLC, B16-F10, A549, MC38, and SVEC4-10 cells were maintained in Roswell Park Memorial Institute (RPMI) 1640 (HyClone, USA) supplemented with 10% fetal bovine serum (FBS) Clarks, Uruguay) and 1% Penicillin–Streptomycin solution (P/S) (Procell, PB180120). THP-1 cells were maintained in RPMI 1640 (HyClone, USA) supplemented with 10% FBS, 0.05 mM β-mercaptoethanol (AMRESCO, 0482), and 1% P/S. HUVEC and HEK-293 cells were cultured in high glucose Dulbecco's Modified Eagle Medium (DMEM) (HyClone, USA) supplemented with 10% FBS and 1% P/S. All cells were cultured in a humidified atmosphere at 37°C with 5% CO₂.

Cell transfection

Viruses were produced by transfection of HEK-293 cells with the pHAGE-puromycin control vector and pHAGE-V5-puromycin expression vectors (carrying *ADAR*-WT or *ADAR*-E912A). *ADAR*-E912A contains an E-to-A amino acid change that abolishes *ADAR*1 editase activity. Transfections were carried out using pLVX-shRNA1 negative control scrambled vectors, pLVX-*ADAR*1 shRNA#1 or pLVX-*ADAR*1 shRNA#2, and the lentiviral packaging plasmids psPAX2 and pMD2G. THP-1 cells were transduced by the virus and then selected using puromycin (3 μg/mL). After 2 weeks of antibiotic selection, the expression of the constructs was verified by reverse transcription-quantitative polymerase chain reaction (RT-qPCR) and western blots.

Reagents and antibodies

2-AP (GlpBio, GC61906), Phorbol 12-myristate 13-acetate (PMA) (MedChemExpress, HY-18739), Recombinant Human IFN-γ (Novoprotein, C014), Recombinant Mouse IL-2 (Novoprotein, P04351), Recombinant M-CSF (Novoprotein, CB34), Recombinant Mouse IFN-γ (Novoprotein, C746), Recombinant Mouse TIM-3 (Novoprotein, CM54), Recombinant Mouse CCL20 (PeproTech, 250–2), Recombinant Mouse GDF15 (R&D Systems, 8944-GD-025), Recombinant Mouse IL-18 Binding Protein Isoform d (Novoprotein, CM45), ShortCut RNase III (NEB, M0245S), poly (I:C) (GlpBio, GC14710).

Anti-*ADAR*1 antibody (Santa Cruz, sc-73408), anti-*ADAR*1 antibody (Santa Cruz, sc-271854), anti-V5 antibody (Invitrogen, R960-251), anti-β-actin antibody (EnoGene, E12-041-1), anti-CD31 antibody (Abcam, ab28364), anti-PKR (phospho T446) antibody (Abcam, ab32036), anti-PKR (phospho T451) antibody (Abcam, ab81303), anti-PKR antibody (ProteinTech, 18244-1-AP), anti-CD8a antibody (Invitrogen, 14-0081-85), anti-EIF2α antibody (ProteinTech, 11170-1-AP), anti-EIF2α (phospho Ser51) antibody (Abmart, TA3087S), anti-J2 antibody (SCICONS, 10010200), anti-CD8a antibody (Cell Signaling Technology, 98941), anti-CD28 antibody (Abmart, TA0014S), anti-CD3 antibody (Invitrogen, 14-0032-82), PE anti-mouse CD8a antibody (Elabscience, E-AB-F1104D), APC anti-mouse Perforin Antibody (BioLegend, S16009B), APC Rat IgG2a, κ Isotype Control (Elabscience, E-AB-F09832E), APC anti-human/mouse Granzyme B Recombinant Antibody (BioLegend, 372204), APC mouse IgG1, κ Isotype Control (Elabscience, E-AB-F09792E), APC anti-mouse/human CD11b antibody (BioLegend, 101212), FITC anti-mouse F4/80 antibody (BioLegend, 123108), Alexa Fluor 488 AffiniPure Donkey Anti-Rat IgG (H+L) (Jackson, 712-545-150), Alexa Fluor 594 AffiniPure Donkey Anti-Rabbit IgG (H+L) (Jackson, 711-585-152).

Experimental animals

Adar knockout in C57BL/6 mouse macrophages was done using TurboKnockout gene knockout technology, and exons four to six of the *Adar* gene were used as conditional knockout regions. Mouse models including *Adar*^{fl/fl} versus *Adar*^{fl/fl}*Lyz2*^{cre} were purchased from Cyagen Biosciences.

Mouse genotyping

We used the One Step Mouse Genotyping Kit (Vazyme, PD101-01) to identify mouse types: *Adar*^{fl/fl} versus *Adar*^{fl/fl}*Lyz2*^{cre}. The primers used were *Adar* (Forward, 5'-CAT CTA ATG AGC TGA GAG GCT GAA -3'; Reverse, 5'-GTG ACT TCT TAC TAA TGT TCT CTG AGC -3') and *Lyz2*^{cre} (Forward, 5'-CCC AGA AAT GCC AGA TTA CG -3'; Reverse, 5'-CTT GGG CTG CCA GAA TTT CTC -3'). The PCR products were identified using 1% agarose gel electrophoresis. Tanon 5200 Multi automatic chemiluminescence/fluorescence image analysis system was used for luminescence detection.

Mouse macrophage extraction, culture, and identification

Mice were killed under anesthesia, and the femur and tibia were collected. HBSS (Procell, PB180323) containing 5% FBS was used to flush out the bone marrow, and single-cell suspensions were made. Cell suspensions were centrifuged at 314g for 5 min at 4°C, the supernatant was discarded, and red cells were lysed using a red blood cell lysis buffer (Beyotime, C3702). Cells were washed using HBSS containing 5% FBS and resuspended in RPMI 1640 supplemented with 10% FBS, 1% P/S, and 20 ng/mL macrophage colony-stimulating factor (M-CSF) for culture. The purity of BMDMs was assessed using flow cytometry.

Western blot

Protein lysates were extracted in RIPA buffer (Beyotime, P0013B) containing protease inhibitors (MedChemExpress, HY-K0010) and phosphatase inhibitors (MedChemExpress, HY-K0021). Protein lysates were quantified, separated by SDS-PAGE gel, transferred onto polyvinylidene difluoride membranes (Millipore, Billerica, Massachusetts, USA), and detected with specific primary antibodies and horse radish peroxidase (HRP)-conjugated secondary antibodies in combination with enhanced chemiluminescence (Vazyme, E411-04). Luminescence detection was performed using a Tanon 5200 Multi automatic chemiluminescence/fluorescence image analysis system.

Tumor xenograft

We used 12–16 weeks old C57BL/6 mice (*Adar*^{fl/fl} vs *Adar*^{fl/fl}*Lyz2*^{cre}) for mouse experiments. Each mouse was injected subcutaneously with 2×10⁶ or 1.5×10⁶ LLC, B16-F10, or MC38 cells. IFN-γ (2.5 μg/mouse) was injected every 3 days after tumor formation. Tumor sizes were measured every 3 days. At the end of the experiments, the mice were killed by anesthesia and photographed for tumor measurement, and the growth of the tumors was measured.

Human cytokine array

Human XL Cytokine Array Kit (R&D Systems, ARY022B) was used to detect 105 soluble human proteins, including cytokines, chemokines, and growth factors in the macrophage-conditioned media. Chemiluminescence was detected on a Tanon 5200 Multi automatic chemiluminescence/fluorescence image analysis system, and ImageJ was used for grayscale analysis.

RT-qPCR

Total RNA was isolated using the MiniBEST Universal RNA Extraction Kit (TAKARA, 9767) according to the manufacturer's instructions. RNAs were transcribed into complementary DNAs using the PrimeScript RT reagent Kit with a gDNA eraser (TAKARA, RR047A). TB Green Premix Ex Taq II (TAKARA, RR820A) was used to perform RT-PCR on an Applied Biosystems StepOne Real-Time PCR system (Applied Biosystems, Darmstadt, Germany). The primers were as follows: human *ADAR* (Forward,

5'- CTG AGA CCA AAA GAA ACG CAG A -3'; Reverse, 5'- GCC ATT GTA ATG AAC AGG TGG TT-3'); human *β-actin* (Forward, 5'- ATT GGC AAT GAG CGG TTC CG -3'; Reverse, 5'- CGT GGA TGC CAC AGG ACT CC -3'); human *CCL20* (Forward, 5'- AAG TTG TCT GTG TGC GCA AAT CC -3'; Reverse, 5'- CCA TTC CAG AAA AGC CAC AGT TTT -3'); human *GDF15* (Forward, 5'- CAA CCA GAG CTG GGA AGA TTC G -3'; Reverse, 5'- CCC GAG AGA TAC GCA GGT GCA -3'); human *HAVCR2* (Forward, 5'- GAC TCT AGC AGA CAG TGG GAT C -3'; Reverse, 5'- GGT GGT AAG CAT CCT TGG AAA GG -3'); human *IFN-γ* (Forward, 5'- GAG TGT GGA GAC CAT CAA GGA G -3'; Reverse, 5'- TGC TTT GCG TTG GAC ATT CAA GTC -3'); human *IL-18* (Forward, 5'- GAT AGC CAG CCT AGA GGT ATG G -3'; Reverse, 5'- CCT TGA TGT TAT CAG GAG GAT TCA -3'); human *IL-18BP* (Forward, 5'- GTG TCC AGC ATT GGA AGT GAC C -3'; Reverse, 5'- GGA GGT GCT CAA TGA AGG AAC C -3'); mouse *Ccl20* (Forward, 5'- GTG GGT TTC ACA AGA CAG ATG GC -3'; Reverse, 5'- CCA GTT CTG CTT TGG ATC AGC G -3'); mouse *Gdf15* (Forward, 5'- AGC CGA GAG GAC TCG AAC TCA G -3'; Reverse, 5'- GGT TGA CGC GGA GTA GCA GCT -3'); mouse *Il-18* (Forward, 5'- GAC AGC CTG TGT TCG AGG ATA TG -3'; Reverse, 5'- TGT TCT TAC AGG AGA GGG TAG AC -3'); mouse *Il-18bp* (Forward, 5'- TCT CCA GCA GTC CCA ACT AAG C -3'; Reverse, 5'- AGG CAG TAC AGG ACA AGG TCA G -3'); mouse *Havcr2* (Forward, 5'- ACA GAC ACT GGT GAC CCT CCA T -3'; Reverse, 5'- CAG CAG AGA CTC CCA CTC CAA T -3'); mouse *Gapdh* (Forward, 5'- CAT CAC TGC CAC CCA GAA GAC TG -3'; Reverse, 5'- ATG CCA GTG AGC TTC CCG TTC AG -3').

Immunofluorescence

Mouse tissue sections or fixed cells were incubated with specific antibodies overnight at 4°C, followed by fluorescently-labeled secondary antibodies for 90 min at room temperature. After 4',6-diamidino-2-phenylindole (DAPI) counterstaining, images were taken using an Olympus LEXT OLS4500 confocal laser scanning microscope.

ELISA

The cytokines of interest were detected in macrophage-conditioned media according to the kit instructions. The following kits were used: Mouse MIP-3α (Macrophage Inflammatory Protein 3 Alpha) ELISA Kit (Elabscience, E-EL-M0013c). Mouse GDF15 (Growth Differentiation Factor 15) ELISA Kit (Elabscience, E-EL-M0604c). Human IFN-γ ELISA Kit (Elabscience, E-EL-H0108c). Mouse TIM-3 ELISA Kit (Camilo, No. 2M-KMLJM219388m). Mouse IL-18 ELISA Kit (Elabscience, E-EL-M0730c). Mouse IL-18 BP ELISA Kit (Elabscience, E-EL-M0739c). A Thermo Scientific Multiskan Sky Spectrum instrument was used for luminescence detection.

5'UTR activity assay

The 5'UTR sequences of *CCL20*, *HAVCR2*, *IL-18*, and *IL-18* mutant were cloned into the pGL3-Control vector.

The fusion plasmids were purchased from GeneCreate Company (Wuhan, China). THP-1 cells were co-transfected with the fusion plasmids and pRL-TK and were then treated with IFN- γ (100 ng/mL) for 24 hours. Cells were collected, and the luminescence intensity of the firefly and Renilla luciferase was measured using a TECAN Infinite 200 PRO microplate reader according to the Dual Luciferase Reporter Assay Kit (Vazyme, DL101-01). The sequences of 5'UTR: *CCL20* (5'UTR: AGA ATA TAA CAG CAC TCC CAA AGA ACT GGG TAC TCA ACA CTG AGC AGA TCT GTT CTT TGA GCT AAA AAC C); *HAVCR2* (5'UTR: ATT TGG AGA GTT AAA ACT GTG CCT AAC AGA GGT GTC CTC TGA CTT TTC TTC TGC AAG CTC C); *IL-18* (5'UTR: CCT TTG CTC CCC TGG CGA CTG CCT GGA CAG TCA GCA AGG AAT TGT CTC CCA GTG CAT TTT GCC CTC CTG GCT GCC AAC TCT GGC TGC TAA AGC GGC TGC CAC CTG CTG CAG TCT ACA CAG CTT CGG GAA GAG GAA AGG AAC CTC AGA CCT TCC AGA TCG CTT CCT CTC GCA ACA AAC TAT TTG TCG CAG ATG GCT CTT TGC TTT CAT TAG (uORF) GAA TAA AG); *IL-18-Mutant* (5'UTR: CCT TTG CTC CCC TGG CGA CTG CCT GGA CAG TCA GCA AGG AAT TGT CTC CCA GTG CAT TTT GCC CTC CTG GCT GCC AAC TCT GGC TGC TAA AGC GGC TGC CAC CTG CTG CAG TCT ACA CAG CTT CGG GAA GAG GAA AGG AAC CTC AGA CCT TCC AGA TCG CTT CCT CTC GCA ACA AAC TAT TTG TCG CAG AGG GCT CTT TGC TTT CAT TAG GAA TAA AG).

Immunohistochemistry

Mouse specimens were fixed in 4% paraformaldehyde and paraffin-embedded. For immunohistochemistry (IHC) staining, the antibodies against CD31 or CD8a were used. Endogenous stained slides were visualized using a microscope (Nikon 90i) with 10 \times and 40 \times objective lens magnification.

Tube formation assay

HUVEC (6 \times 10⁴/well) or SVEC4-10 (6 \times 10⁴/well) cells were suspended in macrophage-conditioned media with or without IFN- γ , CCL20, or GDF15 and then seeded onto Matrigel (BD, 356230) precoated wells of a 96-well plate. After 2–6 hours of incubation, HUVEC or SVEC4-10 cells were stained with 5 nM eBioscience Calcein AM Viability Dye (Invitrogen, USA) for 15 min, and detected at 495 nm by fluorescent microscopy. Tube formation was assessed by estimating the vessel area, the total number of junctions, and the total vessel length using the AngioTool software.

Mouse tumor cell isolation

Mouse tumors were washed in precooled HBSS containing 5% FBS and cut into 1–2 mm pieces. Tumor pieces were digested in 1 mg/mL collagenase I (GlpBio, GC19589) and 5 U/mL DNase I (Beyotime, D7073) for ~1 hour in a 37°C water bath. Digestion was completed when no obvious tissue pieces remained. The cells were filtered using a 70 μ m filter and centrifuged at 600 g for 5 min

at 4°C. The red blood cells were lysed using a red blood cell lysis buffer for 5 min at room temperature. Cells were washed twice in HBSS containing 5% FBS, resuspended in an FBS-containing staining buffer, and counted.

CD8⁺ T cells extraction and culture

Mice were killed under anesthesia, spleens were collected and ground, and the suspension was filtered using a 70 μ m cell filter (Solarbio, F8210). Red blood cells were lysed and cells were resuspended in autoMACS Rinsing Solution (Miltenyi, 130-091-222-1) containing 0.5% FBS. Cells were stained with mouse CD8a (Ly-2) MicroBeads (Miltenyi, 130-117-044) for 10 min at 4°C. Using LS Separation Columns (Miltenyi, 130-042-401), MACS MultiStand (Miltenyi, 130-042-303), and MidiMACS Separator (Miltenyi, 130-042-302), CD8⁺ T cells were collected. Finally, CD8⁺ T cells were seeded into 96-well plates (Corning, 3799) precoated with anti-CD3 antibody (5 μ g/mL). Recombinant mouse IL-2 (20 ng/mL) and anti-CD28 antibody (2 μ g/mL) were added to the cells and incubated for 48 hours.

Flow cytometry

The extracted CD8⁺ T cells were cultured for 48 hours, collected, centrifuged, and plated in a 96-well plate containing macrophage-conditioned media. CD8⁺ T cells were treated with 1 \times PMA/Ionomycin (MultiSciences, 70-CS1001) and 1 \times Brefeldin A (BFA)/Monensin (MultiSciences, 70-CS1002) for 5 hours. The CD8⁺ T cells were resuspended in staining buffer (BD, 554656) and incubated with PE anti-mouse CD8a antibody for 30 min in the dark at 4°C. Cells were fixed and permeabilized using a Fixation/Permeabilization Kit (BD, 554714) and then stained for intracellular targets using specific antibodies. Stained cells were acquired using a BD Accuri C6 Plus Flow Cytometer, and FlowJo was used to analyze data.

CD8⁺ T cells chemotactic assay

We added 600 μ L RPMI 1640 containing 10% FBS or macrophage-conditioned media to the lower chamber of 24-well plates and then placed Boyden chambers (5 μ m) (Corning USA 3421) into the wells. CD8⁺ T cells (1 \times 10⁵) resuspended in 100 μ L RPMI 1640 containing 0.2% FBS were added to the upper chamber, and the cells were cultured for 12 hours. After removing the upper chamber, CD8⁺ T cells were stained by 5 nM eBioscience Calcein AM Viability Dye (Invitrogen, USA) for 15 min and detected at 495 nm by fluorescent microscopy.

Reinfusion of mouse macrophages

We used 12–16 weeks old C57BL/6 mice (*Adar*^{fl/fl}) for experiments. Each mouse was injected subcutaneously with 1.5 \times 10⁶ LLC cells. Starting from the fifth day of LLC cells injection, 3.0 \times 10⁵ macrophages from *Adar*^{fl/fl} and *Adar*^{fl/fl}*Ly2*^{cre} were injected into the tail vein every 3 days. After 11 days of LLC cells injection, IFN- γ (2.5 μ g/mouse) was injected intraperitoneally every 3 days. Tumor sizes were measured every 3 days. At the end of the experiment,

mice were killed under anesthesia and photographed for tumor growth, and tumor sizes were measured.

Author affiliations

¹Department of Pathophysiology, College of Basic Medical Science, China Medical University, Shenyang, Liaoning Province, China

²Graduate Program in Quantitative and Computational Biosciences, Baylor College of Medicine, Houston, Texas, USA

³Department of Bioinformatics and Computational Biology, The University of Texas MD Anderson Cancer Center, Houston, Texas, USA

⁴Department of Systems Biology, The University of Texas MD Anderson Cancer Center, Houston, Texas, USA

Contributors HL and XX conceived of and designed the study, WL, JW, HZhang, GJ, CG, and HZhou contributed to experiments and related data analysis; and YL and HL contributed to the analysis of the public data. XX supervised the whole project and is responsible for the overall content as the guarantor.

Funding This research was financially supported by the National Natural Science Foundation of China (32070790 and 81572777); Liaoning Province Xingliao Talent Program project (XLYC1807223); Outstanding Youth Science Foundation in Liaoning Natural Science Foundation Project (2020-YQ-07); Shenyang Outstanding Young Scientific and Technological Innovation Talent Support Program (RC231006), and the Barnhart Family Distinguished Professorship in Targeted Therapies from MD Anderson Cancer Center. We thank K. Mojumdar for editorial assistance.

Competing interests HL is a shareholder and scientific advisor for Precision Scientific Ltd.

Patient consent for publication Not applicable.

Ethics approval Ethics approval and consent to perform animal studies were approved by the Animal Ethics Committee of China Medical University (CMU2021428 and CMU2022035). All methods were performed in accordance with relevant guidelines.

Provenance and peer review Not commissioned; externally peer reviewed.

Data availability statement Data are available upon reasonable request. All data relevant to the study are included in the article or uploaded as supplementary information.

Supplemental material This content has been supplied by the author(s). It has not been vetted by BMJ Publishing Group Limited (BMJ) and may not have been peer-reviewed. Any opinions or recommendations discussed are solely those of the author(s) and are not endorsed by BMJ. BMJ disclaims all liability and responsibility arising from any reliance placed on the content. Where the content includes any translated material, BMJ does not warrant the accuracy and reliability of the translations (including but not limited to local regulations, clinical guidelines, terminology, drug names and drug dosages), and is not responsible for any error and/or omissions arising from translation and adaptation or otherwise.

Open access This is an open access article distributed in accordance with the Creative Commons Attribution Non Commercial (CC BY-NC 4.0) license, which permits others to distribute, remix, adapt, build upon this work non-commercially, and license their derivative works on different terms, provided the original work is properly cited, appropriate credit is given, any changes made indicated, and the use is non-commercial. See <http://creativecommons.org/licenses/by-nc/4.0/>.

ORCID iD

Han Liang <http://orcid.org/0000-0001-7633-286X>

REFERENCES

- Liddicoat BJ, Chalk AM, Walkley CR. Adar1, Inosine and the immune sensing system: distinguishing self from non-self. *Wiley Interdiscip Rev RNA* 2016;7:157–72.
- Han L, Diao L, Yu S, et al. The Genomic landscape and clinical relevance of A-to-I RNA editing in human cancers. *Cancer Cell* 2015;28:515–28.
- Chen L, Li Y, Lin CH, et al. Recoding RNA editing of Azin1 predisposes to hepatocellular carcinoma. *Nat Med* 2013;19:209–16.
- Peng X, Xu X, Wang Y, et al. A-to-I RNA editing contributes to Proteomic diversity in cancer. *Cancer Cell* 2018;33:817–28.
- Ishizuka JJ, Manguso RT, Cheruiyot CK, et al. Loss of Adar1 in tumours overcomes resistance to immune Checkpoint blockade. *Nature* 2019;565:43–8.

- Mehdipour P, Marhon SA, Ettayebi I, et al. Epigenetic therapy induces transcription of inverted sines and Adar1 dependency. *Nature* 2020;588:169–73.
- Chung H, Calis JJA, Wu X, et al. Human Adar1 prevents endogenous RNA from triggering Translational shutdown. *Cell* 2018;172:811–24.
- Karki R, Sundaram B, Sharma BR, et al. Adar1 restricts Zbp1-mediated immune response and Panoptosis to promote tumorigenesis. *Cell Rep* 2021;37:S2211–1247(21)01325-5.
- Zhang T, Yin C, Fedorov A, et al. Adar1 masks the cancer Immunotherapeutic promise of Zbp1-driven Necroptosis. *Nature* 2022;606:594–602.
- Pittet MJ, Michielin O, Migliorini D. Clinical relevance of tumour-associated Macrophages. *Nat Rev Clin Oncol* 2022;19:424:402–21..
- Lee WS, Yang H, Chon HJ, et al. Combination of anti-angiogenic therapy and immune Checkpoint blockade Normalizes vascular-immune Crosstalk to potentiate cancer immunity. *Exp Mol Med* 2020;52:1475–85.
- De Palma M, Biziato D, Petrova TV. Microenvironmental regulation of tumour angiogenesis. *Nat Rev Cancer* 2017;17:457–74.
- Hanahan D, Weinberg RA. Hallmarks of cancer: the next generation. *Cell* 2011;144:646–74.
- Li X, Liu R, Su X, et al. Harnessing tumor-associated Macrophages as AIDS for cancer Immunotherapy. *Mol Cancer* 2019;18:177.
- Duan Z, Luo Y. Targeting Macrophages in cancer Immunotherapy. *Signal Transduct Target Ther* 2021;6:127.
- Krishna C, DiNatale RG, Kuo F, et al. Single-cell sequencing links Multiregional immune landscapes and tissue-resident T cells in ccRCC to tumor Topology and therapy efficacy. *Cancer Cell* 2021;39:662–77.
- Zhang X, Peng L, Luo Y, et al. Dissecting Esophageal squamous-cell carcinoma Ecosystem by single-cell Transcriptomic analysis. *Nat Commun* 2021;12:5291.
- Sun K, Xu R, Ma F, et al. scRNA-Seq of gastric tumor shows complex Intercellular interaction with an alternative T cell exhaustion trajectory. *Nat Commun* 2022;13:4943.
- Maynard A, McCoach CE, Rotow JK, et al. Therapy-induced evolution of human lung cancer revealed by single-cell RNA sequencing. *Cell* 2020;182:1232–51.
- Sun D, Wang J, Han Y, et al. TISCH: a comprehensive web resource enabling interactive single-cell Transcriptome visualization of tumor Microenvironment. *Nucleic Acids Res* 2021;49:D1420–30.
- Fumagalli D, Gacquer D, Rothé F, et al. Principles governing A-to-I RNA editing in the breast cancer Transcriptome. *Cell Rep* 2015;13:277–89.
- Vitali P, Scadden ADJ. Double-stranded Rnas containing multiple IU pairs are sufficient to suppress interferon induction and apoptosis. *Nat Struct Mol Biol* 2010;17:1043–50.
- Zhong Q, Jenkins J, Moldobaeva A, et al. Effector T cells and ischemia-induced systemic angiogenesis in the lung. *Am J Respir Cell Mol Biol* 2016;54:394–401.
- Das M, Zhu C, Kuchroo VK. Tim-3 and its role in regulating anti-tumor immunity. *Immunol Rev* 2017;276:97–111.
- Acharya N, Sabatos-Peyton C, Anderson AC. Tim-3 finds its place in the cancer Immunotherapy landscape. *J Immunother Cancer* 2020;8:e000911.
- Kim JE, Patel MA, Mangraviti A, et al. Combination therapy with anti-PD-1, anti-TIM-3, and focal radiation results in regression of murine gliomas. *Clin Cancer Res* 2017;23:124–36.
- Zhou T, Damsky W, Weizman O-E, et al. IL-18Bp is a secreted immune Checkpoint and barrier to IL-18 Immunotherapy. *Nature* 2020;583:609–14.
- Bass BL, Weintraub H. An unwinding activity that Covalently modifies its double-stranded RNA substrate. *Cell* 1988;55:1089–98.
- Ota H, Sakurai M, Gupta R, et al. Adar1 forms a complex with Dicer to promote microRNA processing and RNA-induced gene silencing. *Cell* 2013;153:575–89.
- Kang J-I, Kwon S-N, Park S-H, et al. PKR protein kinase is activated by hepatitis C virus and inhibits viral replication through Translational control. *Virus Res* 2009;142:51–6.
- Harashima A, Guettouche T, Barber GN. Phosphorylation of the NFAR proteins by the dsRNA-dependent protein kinase PKR constitutes a novel mechanism of Translational regulation and cellular defense. *Genes Dev* 2010;24:2640–53.
- McAllister CS, Taghavi N, Samuel CE. Protein kinase PKR amplification of interferon beta induction occurs through initiation factor eIF-2Alpha-mediated Translational control. *J Biol Chem* 2012;287:36384–92.
- Okumura F, Okumura AJ, Uematsu K, et al. Activation of double-stranded RNA-activated protein kinase (PKR) by interferon-stimulated gene 15 (Isg15) modification down-regulates protein translation. *J Biol Chem* 2013;288:2839–47.



- 34 Sheng W, LaFleur MW, Nguyen TH, *et al.* Lsd1 ablation stimulates anti-tumor immunity and enables Checkpoint blockade. *Cell* 2018;174:549–63.
- 35 Lee JH, Park EJ, Kim OS, *et al.* Double-stranded RNA-activated protein kinase is required for the LPS-induced activation of Stat1 inflammatory signaling in rat brain glial cells. *Glia* 2005;50:66–79.
- 36 Sugiyama T, Gotou T, Moriyama K, *et al.* Mechanism of inhibition of Lipopolysaccharide-induced interferon-beta production by 2-Aminopurine. *Mol Immunol* 2012;52:299–304.
- 37 von Holzen U, Pataer A, Raju U, *et al.* The double-stranded RNA-activated protein kinase mediates radiation resistance in Mouse embryo fibroblasts through nuclear factor kappaB and AKT activation. *Clin Cancer Res* 2007;13:6032–9.
- 38 Dixon KO, Tabaka M, Schramm MA, *et al.* TIM-3 restrains anti-tumour immunity by regulating Inflammasome activation. *Nature* 2021;595:101–6.
- 39 Vatter KM, Wek RC. Reinitiation involving upstream Orfs regulates Atf4 mRNA translation in mammalian cells. *Proc Natl Acad Sci U S A* 2004;101:11269–74.
- 40 Wolf Y, Anderson AC, Kuchroo VK. Tim3 comes of age as an inhibitory receptor. *Nat Rev Immunol* 2020;20:173–85.
- 41 Hansen JA, Hanash SM, Tabellini L, *et al.* A novel soluble form of Tim-3 associated with severe graft-versus-host disease. *Biol Blood Marrow Transplant* 2013;19:1323–30.
- 42 Ueland T, Heggelund L, Lind A, *et al.* Elevated plasma sTIM-3 levels in patients with severe COVID-19. *J Allergy Clin Immunol* 2021;147:92–8.
- 43 Geng H, Zhang G-M, Li D, *et al.* Soluble form of T cell IG Mucin 3 is an inhibitory molecule in T cell-mediated immune response. *J Immunol* 2006;176:1411–20.
- 44 Ivashkiv LB. Ifngamma: signalling, Epigenetics and roles in immunity, metabolism, disease and cancer Immunotherapy. *Nat Rev Immunol* 2018;18:545–58.
- 45 Sun L, Kees T, Almeida AS, *et al.* Activating a collaborative innate-adaptive immune response to control metastasis. *Cancer Cell* 2021;39:1361–74.
- 46 Todd PA, Goa KLI gamma-1b. A review of its pharmacology and therapeutic potential in chronic granulomatous disease. *Drugs* 1992;43:111–22.
- 47 Mantovani A, Marchesi F, Malesci A, *et al.* Tumour-associated Macrophages as treatment targets in oncology. *Nat Rev Clin Oncol* 2017;14:399–416.
- 48 Love MI, Huber W, Anders S. Moderated estimation of fold change and dispersion for RNA-Seq data with Deseq2. *Genome Biol* 2014;15:550.